Optical Tomography

Christoph Haisch

Institute of Hydrochemistry, Technische Universität München, D-81377 Munich, Germany; email: Christoph.Haisch@ch.tum.de

Annu. Rev. Anal. Chem. 2012. 5:57–77

First published online as a Review in Advance on April 13, 2012

The *Annual Review of Analytical Chemistry* is online at anchem.annualreviews.org

This article's doi: 10.1146/annurev-anchem-062011-143138

1936-1327/12/0719-0057$20.00

Keywords

optical tomography, biomedical imaging, atmosphere, tomography reconstruction

Abstract

The number of applications using optical tomography has significantly increased over the past decade. A literature research providing this term as keyword gives 26 hits for 1990, 719 for 2000, and 9,202 for 2010. With an increasing number of applications, the number of different imaging modalities is also increasing. This review summarizes recent developments in tomographic methods for scattering and nonscattering samples. These two different cases of optical tomography are typically represented by biomedical imaging and atmospheric tomography, representing high- and low-scattering samples, respectively. An essential prerequisite for tomographic analyses is an understanding of light propagation in different media, which allows for the development of specific reconstruction algorithms for the different tomographic tasks.

1. INTRODUCTION

Computer tomography, based on X-ray contrast, and magnetic resonance tomography are well-known tomographic techniques routinely applied in medical diagnosis. Despite their indisputable merits, they have certain limitations: For computer tomography, these include size, costs, and the use of ionizing radiation. Although not as well known, optical tomography (OT) is increasingly relevant in various fields. The possibilities and limitations of novel OT techniques are presented here. Section 2 is devoted to the fundamentals of OT, particularly image-reconstruction and photon-transport calculations. Sections 3–5 present different kinds of OT techniques: emission tomography (Section 3); tomographic techniques for low-scattering samples, particularly for atmospheric measurements (Section 4); and techniques for highly scattering samples, mostly for biomedical applications (Section 5).

The term tomography is composed of the Greek word tomein, meaning to cut or dissect, and the word graphein, meaning to write. Hence, the literal meaning of tomography is the display of plane sections of a steric object. The aim of tomographic imaging is to represent a single image plane taken of a three-dimensional (3D) structure, with the least influence of the adjacent planes. In contrast, projection is the representation of a 3D structure by its properties integrated along one projection axis. An example of a projection technique is the classical medical X-ray imaging. The resulting image represents a superposition of all absorbing or scattering structures along the respective projection axis. Tomographic imaging separately unveils the single layers forming these overlapping projections. Techniques that compose a 3D image from the stepwise analysis of single volume elements (voxels), namely quasi-punctiform analyses, are not considered tomographic here. Thus, confocal microscopy is not included in the tomographic techniques, although it is widely used for 3D imaging (1–3). OT covers the field of techniques suitable for revealing structural and quantitative analytical tomographic information based on optical, spectroscopic methods such as absorption and scattering of light. Limitation to the spectral range from UV to IR is common (4). A special focus in the following discussion is placed on tomographic approaches not only to reveal structural information, specifically, qualitative information on the distribution of a specific contrast agent in the volume of interest, but also to allow for spatially resolved quantification of a specific target substance.

Tomographic techniques can be classified according to several criteria. One is the way the 3D image is composed from several individual measurements. Traditionally, the term tomography was reserved for 3D medical imaging based on multiangle X-ray transmission, as summarized by Van Tiggelen (5). For these techniques, the 3D information is reconstructed using several two-dimensional (2D) transmission images. Optical coherence tomography (OCT) images, by contrast, are reconstructed by combining single axial scans. A more fundamental classification follows the physical effect employed for image generation. The prototype, X-ray tomography, achieves the image contrast from the intensity of transmitted X-ray photons. In the simplest case, resulting in the highest contrast, photons either are transmitted directly without any interaction with the matrix or are absorbed; for both, scattering is negligible. Although this condition can be reasonably assumed for X-ray tomography, it is rarely fulfilled for OT. Atmospheric tomography of a limited area, carried out by IR transmission tomography or differential optical absorption spectroscopy (DOAS; see below), is one of a few examples where light scattering can be neglected. In a general approach, photon diffusion by elastic and inelastic scattering as well as secondary effects, such as fluorescence excitation, must be considered.

2. TOMOGRAPHIC RECONSTRUCTION

Depending on the experimental conditions and the aim of a tomographic approach, the complexity of the mathematical procedure necessary to extract maximum useful content from the measured

data can be tremendous. An all-embracing discussion of reconstruction strategies goes far beyond the scope of this review, but the most common methods are introduced, providing the basis for many others. Concise discussions about tomography-reconstruction algorithms can be found in References 4, 6, 7, and 8.

Tomographic reconstruction is a mathematical challenge that is generally ill posed or ill conditioned. Following Hadamard's (9) definition, a mathematical problem is considered well posed when it provides a unique solution that depends continuously on the data. Ill-conditioned problems are identified by extreme changes in the result in response to minor changes in the input data. Inversion problems are often ill posed or ill conditioned because the solution is not unique or, more commonly, does not depend continuously on the input data.

2.1. Photon-Transport Models

The first step of an OT experiment is to illuminate the sample. If light scattering is negligible, light propagation can be solved by straightforward ray optics, which is not discussed here. For scattering samples, photon transport can be simulated by different models. Numeric models are usually based on Monte Carlo simulations (10–13). Simulated photons are launched onto the sample, and depending on the assumed local optical properties, the photons are randomly scattered or absorbed. Simulation with a sufficiently large number of photons ($>10^4$ photons) (14) yields reliable photon distributions even for complex samples. The major disadvantage of Monte Carlo simulation is that it does not allow for inversion; that is, it is not suitable for extraction of optical properties from a measured or simulated photon distribution. For this reason, analytical photon-transport models have to be employed. The basis of these models is a continuity equation for the photons, the radiative transfer equation, which physically represents the conservation of energy:

$$\boldsymbol{v} \cdot \nabla L(\boldsymbol{r}, \boldsymbol{v}) + (\mu_a + \mu_s) L(\boldsymbol{r}, \boldsymbol{v}) = \mu_s \oint_{S^2} L(\boldsymbol{r}, \boldsymbol{v}') p(\boldsymbol{v}, \boldsymbol{v}')\, d\boldsymbol{v}' + \frac{1}{4\pi} S(\boldsymbol{r}),$$

with $\boldsymbol{r} \in \Omega$ and where Ω is the region of interest, $L(\boldsymbol{r},\boldsymbol{v})$ is the photon radiance at location $\boldsymbol{r}$ in the direction of the unit vector $\boldsymbol{v}$ [W·mm^{-2} sr^{-1}], $S(\boldsymbol{r})$ is the isotropic source (W·mm^{-2}), μ_s is the scattering coefficient (mm^{-1}), and μ_a is the absorption coefficient (mm^{-1}). The scattering-phase function $p(\boldsymbol{v},\boldsymbol{v}')$ gives the probability that a photon coming from the direction $\boldsymbol{v}'$ is scattered into the direction $\boldsymbol{v}$ (15, 16). However, the complexity of this equation makes it nearly impossible to find a solution. For strongly scattering matrices with $\mu_s \gg \mu_a$, this equation can be simplified to the photon-diffusion approximation, which is

$$\frac{\partial L(\boldsymbol{r}, \boldsymbol{v}, \boldsymbol{r})}{\partial \boldsymbol{x}} + \mu_a \cdot L(\boldsymbol{r}, \boldsymbol{v}, \boldsymbol{t}) - \nabla \cdot [\mathrm{D} \nabla L(\boldsymbol{r}, \boldsymbol{v}, \boldsymbol{t})] = \frac{1}{4p} S(\boldsymbol{r}, \boldsymbol{t}).$$

Here, the diffusion coefficient D and the reduced scattering coefficient μ_s', respectively, are represented as

$$\mathrm{D} = \frac{1}{3(\mu_a + \mu_s')}$$

and

$$\mu_s' = (1 - g)\mu_s,$$

where g is the scattering asymmetry factor.

Common numeric solutions employ the finite-element method, which fills the volume of interest with a mesh of small-volume elements and solves the diffusion equation for them (17, 18).

A special case of the finite-element method is the finite-difference approach, where the continuum equation to be solved is discretized, thus approximating the derivatives by a difference quotient (19).

2.2. Radon Transformation

One of the oldest, although still extensively used, reconstruction algorithms is based on the Radon transformation (RT) (20). This transformation determines the integral of the function $f(x,y)$, which is defined within a large disk, along all projections through the plane defined by the disk. Thus, the RT exactly represents a classical tomographic experiment, where a sample is *trans*-illuminated under different angles, and the transmitted light, that is, the projection under these angles, is measured (**Figure 1**). In the case of OT, the function $f(x,y)$ represents the spatial distribution of the optical absorption and scattering coefficient $\mu(x,y)$. After parameterization of the projection line, the RT can be written in the following form:

$$Rf(r,\Theta) = \int_{-\infty}^{\infty} f(r\cos a + s\sin a, r\sin a - s\cos a)ds\,.$$

From the projection-slice theorem (21), an infinite number of projections taken under an infinite number of angles is theoretically deduced to reveal a perfect reconstruction of any possible structure (22). This deduction implies that inversion of the RT for real-world data concludes in reconstruction with essentially limited precision.

Depending on the kind of sample to be imaged and the tomographic approach chosen, the angular coverage and the projection density may be very limited. Whereas medical X-ray tomography operates with a high number of projections plus full angular coverage (23), other techniques, for example, in atmospheric tomography, are limited for practical reasons to only two measuring positions covering less than 60° of the full circle. Depending on these prerequisites, on the a priori knowledge on the structure of the sample to be reconstructed, and on the required precision, different reconstruction approaches have to be chosen. Three basic approaches are presented here.

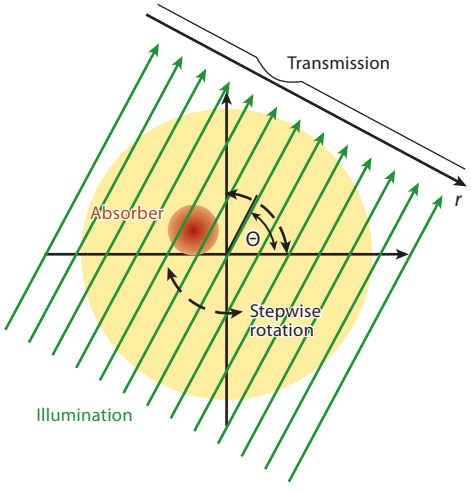

Figure 1

Principle of the Radon transformation.

2.3. Fourier Transform–Based Back-Projection

Fourier transform (FT)-based back-projection is based on the projection-slice theorem cited above (22). It states that the following two operations are equivalent: First, a one-dimensional (1D) FT is applied on the RT of a function $f(x,y)$. Second, the 2D FT of the same function $f(x,y)$ is calculated, and from the result, a slice is taken through its origin and parallel to the projection line of the RT. Hence, back-projection can be achieved by the inverse 2D FT of the projection slices. However, inverse FT requires a polar to Cartesian grid conversion, which may induce artifacts (24).

2.4. Filtered Back-Projection

The direct reversal of the projection described by the RT is the back-projection of the measured projection signals on the projection axis by homogeneous distribution on all pixels along the projection axis. This back-projection is repeated for all projection angles, while the values are integrated over all projections for each single pixel. Although this approach roughly reveals the structure of optical inhomogeneities, particularly if they feature step gradients, the images generated this way are blurry as a result of the implied point spread function $1/r$ of this approach (where r is the distance from the projection point). For the filtered back-projection, this point spread function is convoluted by a convolution kernel, which depends on the specific imaging task (25). The filtered back-projection can be performed with limited computational resources; thus, it is very fast. The particular advantages and disadvantages of filtered back-projection as well as alternatives are discussed in References 26 and 27. A similar approach is filtered back-propagation, as described and compared with the back-projection approach in References 28 and 29.

2.5. Algebraic Reconstruction Technique

The algebraic reconstruction technique (ART) comprises a class of iterative reconstruction algorithms introduced by Gordon et al. (30) to reconstruct electron-microscopy and X-ray photography data. As the authors stated in their initial publication, this technique is particularly suitable for tomographic problems featuring very limited angular coverage. The first step of the iteration is a homogeneous distribution of the average absorption loss to all pixels. Deviation from this average energy loss, integrated along one projection axis, from the value measured is taken as a first correction for all pixels along this projection. In the next iteration, the same is carried out along another projection line, taking the result of the first step as the starting value. The process is repeated for all projection angles available and then restarted with the first one. This approach is computationally straightforward and can be performed rather quickly (31).

3. EMISSION TOMOGRAPHY

Typical samples for optical emission tomography are plasmas and flames because they emit optical radiation. A common aim in this field is spatially resolved temperature measurements (32). A typical setup for 3D plasma monitoring based on optical emission generally consists of a spectrally resolved detection that can be rotated around the plasma and adjusted in height (**Figure 2**) (33). Although axial symmetry is assumed in most cases (34), some reconstruction algorithms are optimized for asymmetric flames (35). As discussed by Correia et al. (32), precise temperature and relative population calculations as required for analytical plasma sources (36, 37), which in turn require that the reconstruction algorithm take reabsorption into account (32). A common inversion algorithm for this task is the Abel inversion (38, 39), which is also commonly applied for laser-induced

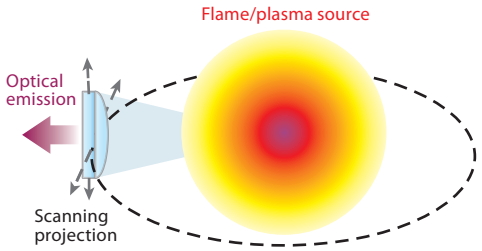

Figure 2

Principle of optical emission tomography.

plasmas (40). Many publications deal with the optimization of analytical plasma sources, such as inductively coupled plasmas (41), radio frequency plasmas (42), or arc discharge plasmas (43), and technical plasma sources (44).

4. TOMOGRAPHY IN GASES AND LOW-SCATTERING MEDIA

OT for atmospheric measurements, similar to conventional gas absorption spectroscopy, allows for the analysis of the local trace gas concentration, analogous to most other analytical applications of OT. Beyond quantitative or semiquantitative analyses of absorbing trace gases, the atmosphere's optical properties, namely local light absorption and scattering, are of major interest, as they influence the global radiation balance (45). Atmospheric analysis often covers large-volume areas and areas that are not readily accessible for in situ sampling and analysis. An extreme example of a large-volume area is the worldwide mapping of trace gases such as ozone; the second may include areas such as volcanic emissions (46), forest fire emissions (47), or noxious industrial emissions (48). On the other end of the scale, spatial patterns of interest can be as small as an indoor environment of a few meters. Outdoor applications are often intended to monitor spatial distribution following local emission, such as high-traffic roads, domestic heating, and industry or power plants, but they may also target large areas. An extreme case is worldwide monitoring of different atmospheric constituents, which is carried out from satellites. An overview of a wide range of tomographic techniques for atmospheric monitoring can be found in Reference 49.

Early approaches of atmospheric tomography were inspired by classical X-ray concepts. Byer & Shepp (50) discussed a radial symmetric setup with a laser source in the center. The laser beam is directed to one of many convex mirrors placed on a circle around the area of interest. Each of the mirrors also includes a light detector. The mirror defocuses the light such that the complete area enclosed by the mirrors is illuminated and light transmitted through this area is detected by the detectors at the opposite side, thus revealing optical transmission along nearly as many lines of sight as the number of mirror/detector systems (the number is slightly lower owing to the limited acceptance angle of the detectors). The authors estimated that a spatial resolution of 10 m inside a 2,000-m-diameter circle would require 314 mirror/detector pairs. Despite the ingenuity of this approach, no practical realization of the concept can be found in the literature. Instead, the established atmospheric tomographic methods require reconstruction approaches that are different from other tomographic methods. Some reasons for this include the following:

1. A limited number of beams may be targeted through the volume of interest.
2. A limited number of viewing angles are available onto the relevant volume (e.g., monitoring of emission plumes only from Earth's surface, that is, from below but not from above).

3. Smooth concentration gradients rather than steps, as are common in, for example, medical imaging, result.
4. Multiple light scattering is mostly neglected.

An essential tool for atmospheric tomography is the modeling of the phenomena to be observed. On the one hand, it may reveal qualitative information on the distribution of gaseous or particulate atmospheric constituents; on the other hand, these models are necessary to assess the validity of tomographic reconstruction algorithms, particularly if quantitative information is required. Wolfe & Byer (51) have carried out the latter, for instance, concerning Byer & Shepp's early discussion on atmospheric tomography, discussed above (50).

Atmospheric diffusion of this kind of emission results in so-called Gaussian plumes. Seinfeld & Pandis (52) provide a detailed discussion and mathematical description of the underlying principles. The dominating physical effect that is responsible for the dissipation of the initial distribution in atmosphere is not molecular diffusion, but rather turbulent mixing of gas masses, commonly attributed to atmospheric diffusion. When imaging a point source that emits a single puff of the analyte gas, diffusion of the puff depends on the ratio of its size to the size of the turbulent eddies. Eddies significantly larger than the plume tend to transport it intact, whereas eddies smaller than the plume disperse it. Thus, over time and with increasing diffusion, increasingly larger eddies become effective as dispersive forces. Feeding the initial conditions for a specific tomographic question into such dispersion models reveals the plume shape that can be expected from a certain emission and thus facilitates tomographic reconstruction. Typical examples are temporally continuous or short-time emission from a point source, such as a stack, or 1D sources such as roads, or 2D emitters as found, for instance, in biomass assessment (53, 54). Three different techniques are commonly employed for atmospheric tomography.

4.1. Open-Path Absorption Gas-Phase Tomography

The starting point for the discussion of gas-phase tomography is the analog to classical X-ray tomography, optical transmission tomography: An optical emitter is placed on a side of the sample volume, while a detector is positioned on the opposite side (**Figure 3**). The measurement is the transmitted optical energy.

Fischer et al. (55) discussed a straightforward realization of this concept for spatially and time-resolved gas-phase analysis. They installed a system of 28 open light paths in an indoor space measuring 7 m by 9 m by 11 m. By rapidly switching between the different light paths and sequentially recording the corresponding optical absorption, they retrieved the line-integrated concentration of CH_4, which was employed as a test gas. For control purposes, 28 short (0.5-m) optical path sensors were distributed over the same space. Both techniques had a time resolution in the range of few seconds, thus rendering them suitable for time-resolved monitoring of the gas diffusion inside the room. Reconstruction was carried out by a combination of ART with an algorithm named smooth basis function minimization, which assumes the concentration profile as a combination of a few Gaussian plumes (56). Yan et al. (57) compared similar reconstruction algorithms, based on Gaussian plumes and polynomial fit of the plumes, and found very similar results. Verkruysse & Todd (58) presented a very similar experimental setup and compared different reconstruction algorithms. Wu et al. (59) demonstrated that an open-path FTIR is suitable not only for gas analysis, but also for aerosol-sized measurements, on the basis of Mie theory.

Flame and plasma monitoring, as discussed above, can also be carried out by optical transmission tomography (47). In their publication, Baum et al. (47) described a simultaneous analysis of gaseous and particulate flame emission. Gases are identified by their specific absorption spectra, whereas

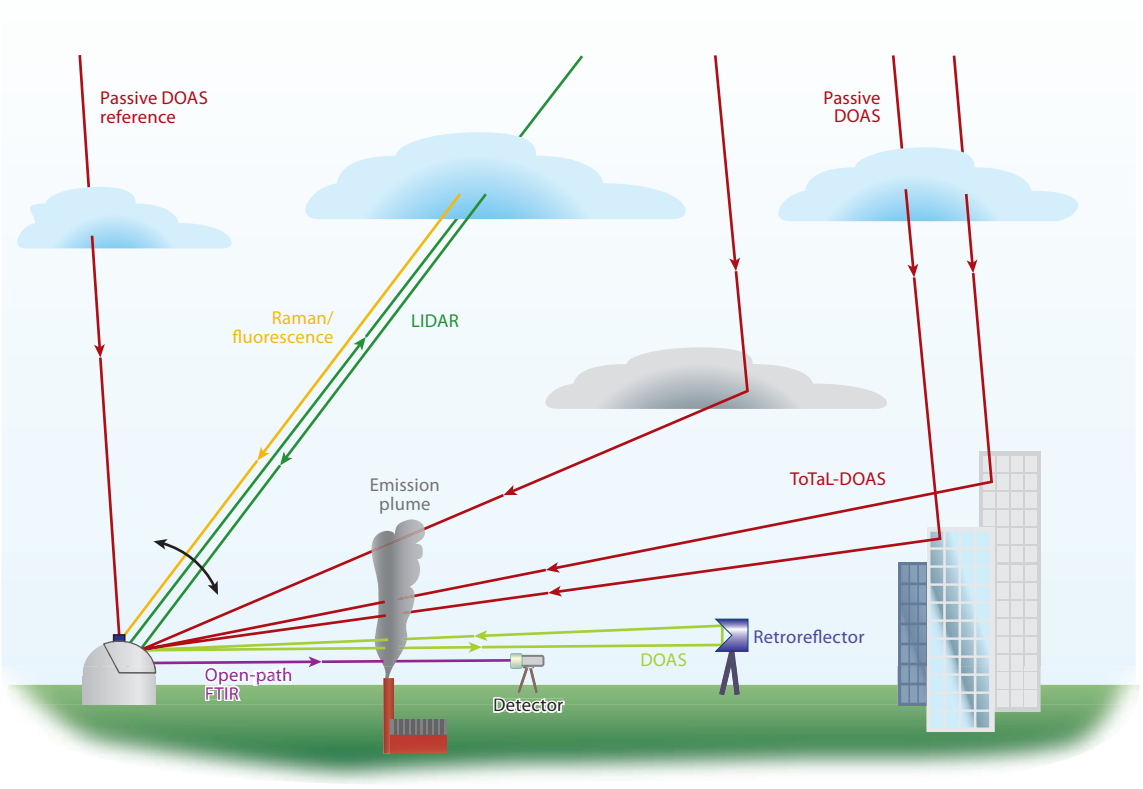

Figure 3

Different methods of optical tomography in low-scattering media. Abbreviations: DOAS, differential optical absorption spectroscopy; FTIR, Fourier transform IR; LIDAR, light detection and ranging; ToTaL, topographic target light.

soot particles are represented by a broad absorption background. The experimental setup is a classical RT tomography: An IR absorption spectrum from 800 cm^{-1} to 4,500 cm^{-1} is detected for each line of sight.

4.2. Differential Optical Absorption Spectroscopy

In its original form, DOAS reveals the integrated optical absorption by the atmosphere between two points separated by distances ranging from tens of meters to kilometers. On one side, a light source and a spectrometer as detector are positioned; the other end of the absorption light path is defined by a retroreflector. As light source, a natural (passive DOAS) or artificial (active DOAS) continuum source is employed, sending a collimated beam to the reflector. A certain range of the optical spectrum is detected simultaneously, allowing for simultaneous detection of one or more components. Most instruments operate in the UV and visible spectral range, which determines the selection of gas components accessible. Typical atmospheric target molecules are trace gases such as ozone, NO_x, SO_2, and numerous hydrocarbons, with sensitivities of parts per trillion (60).

As mentioned above, a single DOAS experiment reveals only the optical absorption and, hence, the analyte concentration, integrated along the complete optical axis. To perform DOAS tomography, a set of retroreflectors has to be placed around the region of interest. Each corresponding light path is then probed consecutively by moving the beam from one retroreflector to the next. However, employing several reflectors but only a single emitter/detector position attains no tomographic resolution owing to the missing axial resolution. A typical example is presented by Pundt (61), who placed two DOAS systems on opposite sides of a road with a distance of 160 m; the reflectors were placed approximately 700 and 800 m down the road, with one on each side. Each of these reflector positions was equipped with four individual reflectors in different heights from 0 to 40 m above street level. With these eight reflectors, 16 different light paths were possible, allowing the reconstruction of a vertical 2D absorption map across the street. The target compound in this campaign was NO_2. The same research group also proposed the use of DOAS tomography for indoor applications, employing three DOAS instruments and several mirrors to cover an entire room measuring 10 m by 15 m (62). From the results, they extrapolated a sensitivity of a few parts per billion for the detection of different trace gases such as NO_2 and SO_2, among others, present in a plume of 600 m. Sensitivity could be better for larger plumes, owing to the larger absorption lengths (63). A typical field application of the same concept is the laterally resolved monitoring of CO_2 emissions from a volcano (64). Reconstruction was based on an iterative algorithm assuming a maximum number of 10 Gaussian emission sources. Sensitivity was no major issue in this work, as CO_2 concentrations were in the range of 1,000 ppm (mass) and more.

In a passive DOAS, the artificial light source is replaced by the Sun, which also renders the retroreflectors unnecessary (**Figure 3**). For tomographic purposes, multiaxis (MAX)-DOAS systems are particularly suitable (65). Whereas common passive DOAS systems primarily analyze the vertical column to the zenith, MAX-DOAS measures the signal under various angles to the zenith. For lower azimuth angles, the scattered photons are detected after passing different distances through atmosphere, thus allowing for the deconvolution of atmospheric layering (66).

For tomography, a MAX-DOAS can be operated in a so-called topographic target light scattering (ToTaL) mode. The major difference from conventional DOAS is the application of reflective surface structures instead of retroreflectors (67). As proposed by Frins et al. (67), the large number of such reflectors enables tomography with high spatial resolution. For quantitative analysis, optical absorption has to be taken into account not only of the light path between the reflecting structure and the detector, but also of the light path through the atmosphere to the reflector. This effect can be corrected for by measuring first the light incident directly from the zenith (reference) and then the reflected light. The difference between these two signals represents the absorption along the measuring leg. Despite this promising approach, large-scale tomographic applications have not yet been described in literature. However, sensitivities down to the parts-per-billion level were demonstrated for SO_2 (68). The practical challenges and limitations specific to atmospheric tomography, namely the limited number of projections and angular coverage, as well as the subsequent consequences are discussed in Reference 46.

4.3. Light Detection and Ranging

Similar to DOAS, light detection and ranging (LIDAR) measures an integrated absorption along a free optical path. However, the detected photons are back-reflected not by a solid target, but rather by particles and molecules in the light pass. Analogous to the name-giving RADAR, spatial resolution along the optical axis is achieved by a time-resolved detection of the backscattering signal. Lim et al. (69) described the basic operating principles and reviewed the current state of a very specific application of LIDAR, biomass assessment (70). Tomographic LIDAR is carried out

by angularly scanning the beam (71). Image reconstruction is straightforward due to the inherent depth resolution (and thus is not discussed here, as most LIDAR applications are not related to chemical analysis but rather to structural imaging). For analytical purposes, LIDAR operates in a differential mode, analogous to DOAS; in other words, the analysis is carried out at a minimum of two wavelengths, beyond which certain LIDAR modes give rise to more selective data than optical absorption. Although not all these techniques have been used in a tomographic mode, they are presented here as potential tomography tools. In Raman-LIDAR (72), the backscattered signal is detected not only on the emission wavelength, but also on several other Stokes-shifted wavelengths or a continuous section of the Stokes spectrum, allowing for selective gas (73) and aerosol analysis (74, 75). As opposed to the early experiments on Raman-LIDAR, daytime use is now possible without being hampered by background radiation. Another highly selective Raman mode is based on the atomic fluorescence of sodium, potassium, and iron, and it reveals temperatures in the mesopause region. Temperatures are deduced from thermal line broadening of the fluorescence lines. Polarization analysis of the LIDAR signal can be employed to analyze backscattering aerosol particles (76, 77). Gurdev et al. (78) reviewed in detail the possibilities and requirements of applying the LIDAR principle for conventional Radon-type tomography, where the sample is illuminated from two opposite sides. They concluded that, under certain conditions, reconstruction would be straightforward for such a technique.

5. TOMOGRAPHY IN HIGHLY SCATTERING MEDIA

5.1. Optical Projection Tomography

In biomedical applications, optical imaging and tomography give access to valuable functional information on physiology and structures. However, strong optical scattering hampers unambiguous identification of photon pathways through the sample, which is required for straightforward imaging. Although optical projection tomography (OPT) is a relatively new technique that has not been routinely established, it is discussed here because, of all the techniques presented in this review, it most resembles classical X-ray tomography. For OPT, the sample is enclosed into a vertical cylindrical vessel a few centimeters in diameter, and a light beam focuses on the sample in a narrow cone (79). The light transmitted through this line is projected by a set of microscope lenses onto a camera chip. The tomographic section is generated by rotating the sample around the center axis of the sample cylinder in 400 separate steps. Based on back-projection reconstruction algorithms, OPT reveals spatial resolution superior to that of micro-MRI (magnetic resonance imaging) down to tenths of a micrometer (80, 81). OPT also employs the many colored and fluorescent dyes that have been developed for tissue-specific or gene-specific staining (82), which becomes particularly important for visualizing the 3D shapes of specific organs. With a similar setup, a so-called OPT microscope, which can be operated in absorption and polarization modes, makes possible 3D cancer cell imaging and identification after specific labeling with an absorption dye and polarizing nanorods (83). The fluorescence-based imaging mode is also known as emission OPT, operating with the same instrumental setup (81, 84).

5.2. Laminar Optical Tomography

A slightly larger penetration depth is accessible with laminar optical tomography (LOT) (**Figure 3**). LOT is based on the detection of light emerging out of a strongly scattering sample in different distances from a point illumination source. From this distance, light that propagates deeper into tissues can be distinguished from light originating from the surface, thus providing

depth sensitivity. Employing an accurate light propagation model and scanning over the sample surface, image-reconstruction algorithms can deliver 3D images of hemodynamics with high spatial accuracy (85). Ouakli et al. (85) combined LOT with intrinsic optical imaging to analyze the spinal cord activation of rats. For some applications, LOT is also suitable for noncontact measurements (86). As the experimental setup is relatively simple and versatile, hyphenation with other techniques is feasible, for instance, with OCT (see below) (87). The physical effect underlying LOT can also be exploited for fluorescence tomography (FlT) (87).

5.3. Diffuse Optical Tomography

Diffuse optical tomography (DOT) is suitable for samples larger than those used in OPT and LOT (88). DOT is based on time-resolved measurements. The migration time of a single photon reveals the optical path length, which, again, depends on the number of scattering events the photon experienced, but without imparting the photon's trajectory. Time-resolved detection of a short (femtosecond) photon pulse gives rise to three different temporal regimes. For a strongly scattering matrix, such as human tissue, the number of instant, nonscattered, or ballistic photons is very low. The largest fraction is delayed by less than 3 ns for scattering values of $\mu_s = 0.5$–$1.5\ \mathrm{cm}^{-1}$ and a diameter of the test volume of 15 cm; few photons arrive after $\geq$4 ns. These sample parameters represent typical medical samples (89). The typical interaction volume favors not only applications such as small animal tomography (90), but also brain imaging (91).

All three photon fractions are suitable for imaging. Farsiu et al. (92) presented a detailed discussion of ballistic imaging in comparison with diffused imaging. The most common approach is based on the detection of the second fraction. However, most DOT setups are operated in a frequency domain mode, rather than a pulsed mode. In this mode, the sample is illuminated with a high-frequency-modulated continuous-wave laser, and the photon-diffusion time can be deduced from the phase shift between illumination and detection (93). Simultaneous measurement of the signal intensity and phase at many different projections allows for a spatially resolved analysis of scattering and absorption properties, which is required for quantitative analyses and thus assessment of functional parameters such as total hemoglobin and hemoglobin oxygenation (88, 94). Tomographic reconstruction requires stepwise illumination and detection on one plane but under many different angles, resulting in a typical Radon transform (95). The best performance of such systems can be achieved by a simultaneous detection of scattered photons under many angles, as demonstrated by Jiang & Zhang (96). As shown by Proskurin (97), late-arriving photons, that is, photons undergoing extreme scattering, feature special properties. According to his calculations, late photons leak out of a scattering phantom (parameters as described above) approximately 4 ns after the femtosecond laser pulse. Multiple scattering leads to a complete loss of information on its origin in such a way that these photons seem to be emitted homogeneously inside the sample volume.

5.4. Fluorescence Tomography

Although FlT is an emission method, it can be considered a special case of DOT, as both are carried out in a similar way (98). Many FlT systems are suitable for both DOT and FlT. However, reconstruction is complicated by the fact that the photon-migration time through the medium is convoluted by the fluorescence lifetime. Hence, specific reconstruction algorithms are required to employ DOT in either a time or frequency domain mode (as discussed in Reference 99). The measured fluorescence lifetime can be employed as an additional information channel. For FlT,

usually specific or unspecific labels are employed; autofluorescence detection of biological samples is an alternative.

In terms of fluorescence microscopy, FlT can be carried out by two-photon fluorescence to suppress background fluorescence. Image generation by fluorescence emission can be improved by optical clearing, a procedure in which tissue specimens are made optically transparent via perfusion with fixing, dehydrating, and clearing agents, while the fluorescence properties remain unchanged. This approach is suitable for tomographic imaging of small cells such as those found in isolated tumors (100).

5.5. Optical Coherence Tomography

OCT is a tomographic technique suitable for the imaging of surface layers of highly scattering, nontransparent samples, as probing is based on backscattered photons. Basically, it comprises a short-coherence light source and an interferometer with one well-defined reference arm and a probe arm that is directed into the sample (**Figure 4**). Back-reflected photons from inside the sample can interfere with the reference beam only if they travel the same optical path length as the reference beam. A short-coherence light source is required to eliminate the common ambiguities of laser interferometry. An overview of the technique can be found in References 101 and 102. Fourier-domain OCT employs a white-band near-IR light source in combination with spectroscopic detection, which, after Fourier transformation, reveals the complete depth information simultaneously (103, 104). Spatial resolution is in the range of a few micrometers and penetration

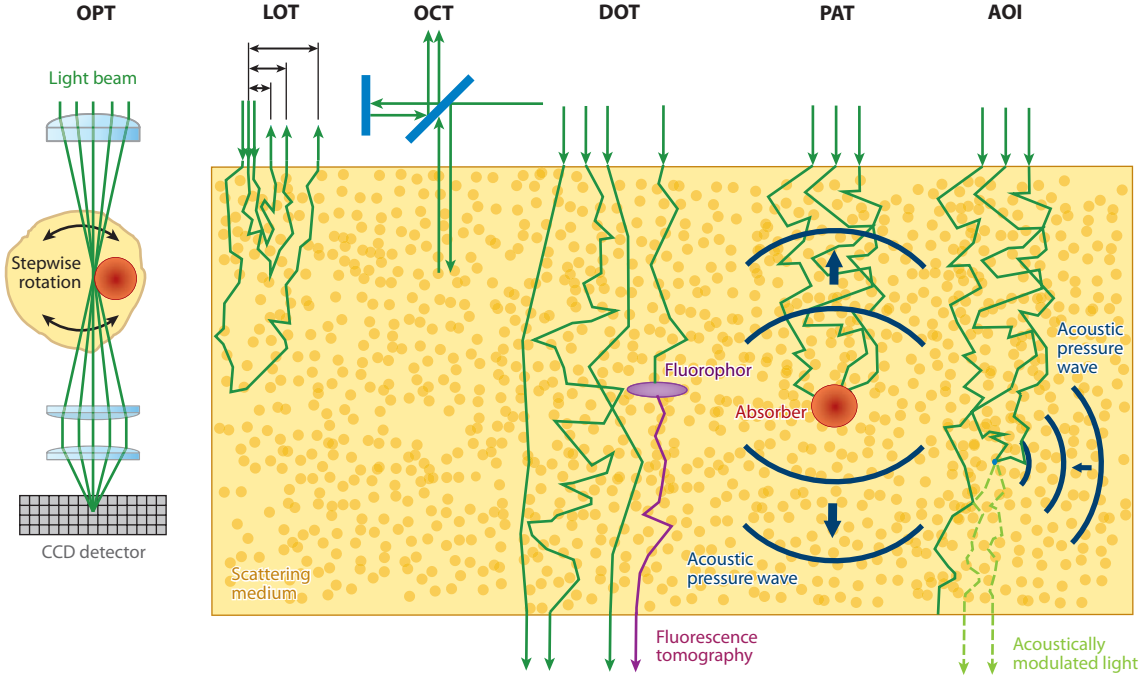

Figure 4

Different methods of optical tomography in low-scattering media. Abbreviations: AOI, acousto-optical imaging; CCD, charge-coupled device; DOT, diffused optical tomography and fluorescence tomography; LOT, laminar optical tomography; OCT, optical coherence tomography; OPT, optical projection tomography; PAT, photoacoustic tomography.

depth also reaches up to a few millimeters (105). As summarized by Roth et al. (106), OCT can also be used in a polarization mode. In medical samples, depolarization of the scattered light detected by the OCT gives rise to muscle-fiber orientation and birefringence, which is related to, for instance, glaucoma diagnosis. Another possibility is a Doppler mode, allowing for spatially resolved flow velocity measurements (107).

Interest in OCT is continuously growing, as can be deduced from the number of publications. In 2000, the ISI Web of Science listed 191 publications with the keywords "optical coherence tomography" in the title; in 2010, 888 papers could be found. However, the best part of the corresponding research is devoted to improved spatial and temporal resolution, particularly for biomedical applications, whereas the number of applications for chemical analysis is limited. Drexler and colleagues (108) demonstrated on a layered sample the possibility of extracting optical absorption information based on frequency-domain OCT and based on proper calibration. Among the very few applications beyond biomedicine, OCT was employed to assess paper porosity (109), to monitor the growth and detachment of biofilms (110, 111), and to analyze pearls and pearl treatment (112).

5.6. Acousto-Optical Imaging

Acousto-optical imaging (AOI) is a special case of DOT where scattered photons, passing a specific volume element, are temporarily modified by a focused acoustic field, which results in a phase and frequency shift of diffuse transmitted photons (**Figure 4**). Three physical effects are generally considered to influence the modulated light transmitted through the acoustic field (113, 114): The ultrasound (US) pressure locally modulates the density of the medium, thus modulating the local refractive index. This effect does not require coherent light to be detected; however, this effect is assumed to be too weak to be detected experimentally (115). The second effect is the displacement of the scatterers by the acoustical field, which influences the path length of the scattered photons. The effect accumulates along the complete path for multiple scattering.

Selective detection of the modulated light allows for the identification of the photons that traveled through the specific volume element. Three-dimensional imaging is carried out by scanning the focus over the volume of interest. The selectivity of AOI is determined by the selectivity of the optical method, whereas spatial resolution is limited by the focused US field. The technique is particularly suitable for bio- and biomedical imaging because optical scattering coefficients in these tissues are generally two to three orders of magnitude larger than are the US scattering coefficients (116). Pure US imaging reveals structures of different mechanical properties, whereas optical absorption contrasts are suitable for a functional analysis of physical properties such as local oxygen saturation or total hemoglobin concentration. Spatial resolution can be calculated to be significantly higher than standard DOT because the mathematical inversion is well posed (117).

As opposed to other experiments and considerations, Bal & Schotland (118) discussed an approach for quantitative analysis based on AOI according to the evaluation of incoherent measurement. Different approaches for the detection of the AOI signal can be found in the literature, ranging from simultaneous speckle detection by cameras using CCDs (charge-coupled devices) (119) or Fabry-Pérot interferometry (120), to interferometric detection based on photorefractive crystals (121). AOI is particularly suitable for strongly light-scattering samples with low US absorption. Consequently, photons are tagged all along the propagation axis of the US, inducing disambiguates in the AO image. To overcome this limitation, the use of a frequency-chirped modulation of the US frequency in combination with heterodyne detection was proposed, thus encoding depth information by the beat frequency (122, 123). Another approach is the

combination of AOI with OCT, which results in a remarkable resolution in the millimeter range (113).

5.7. Photoacoustic Tomography

Photoacoustic (PA) tomography (PAT) occupies a special position among the OT methods, because the tomographic information, namely the spatial resolution, is revealed by an acoustic rather than an optical signal and light is employed to excite this acoustical signal. Although the PA effect can be excited by modulated as well as by pulsed optical radiation, only the pulsed-light approach is discussed here, as it is more suitable for tomographic imaging. For pulsed-light PAT, the sample of interest is illuminated by monochromatic optical radiation (**Figure 4**). The absorption of a short laser pulse in a medium leads to the generation of a wideband thermoelastic pressure wave, which propagates through the medium with the corresponding speed of sound (16, 124). Knowing the speed of sound in the medium and the time delay between optical excitation and the detection of the signal on several positions at the sample surface reveals the spatial distribution of the absorbing structure. Patel & Kerl (125) reported the first experiments on this PA modality for liquid measurements. Because the laser pulse is shorter than both the stress relaxation time (stress confinement) and thermal diffusion time out of the illuminated volume element (thermal confinement), quantitative and spatially resolved measurements are possible. Nowadays, optical excitation is invariably carried out by lasers with typical pulse widths in the range of a few nanoseconds. The PA signal depends on several factors: local optical intensity, local optical absorption, and several material properties such as thermal expansion coefficient, the specific heat capacity at constant pressure, and the speed of sound. The PA signal depends primarily on local optical absorption and intensity, making it insensitive to light scattering. However, as scattering influences local light distribution, quantitative analysis by PAT is a challenging task in real-world samples (126).

Recent overviews of the field were presented by Xu & Wang (127), Wang & Wu (16), and Wang (128). The detection of the US signals induced by the PA effect is conventionally carried out by piezo-active sensors of different shapes and sizes. Using a single pressure transducer, only a single depth profile can be detected. Scanning of the detector and, in most cases, the excitation light source over the sample is necessary (e.g., References 129 and 130). The advantages of this detection scheme are its instrumental simplicity and flexibility. Miniaturization is possible down to the size where the PA instrument can be integrated into an intravascular endoscope with a diameter of a few millimeters (131). Here, the line of vision radially points outward, and a disk-shaped 2D slice around the endoscope axis is generated by rotating the device around this axis. The third dimension is probed by stepwise shifting of the endoscope's position.

When the US transducer elements are grouped into arrays, a complete 2D image can be generated without moving the sensors (e.g., Reference 132). These sensor arrays can be shaped according to the application. Oraevsky et al. (133) designed a semicircular sensor array for breast cancer screening, whereas Manohar et al. (134) designed a planar sensor array for the same application. The PA signal generated by a short laser pulse is a wideband signal, covering a frequency range up to several hundred megahertz. This kind of signal can be detected using commercial US transducers as are employed for medical US echography. Instead of sending a US pulse into the medium and obtaining a time-resolved detection of the pulse echo, the US is generated in the medium via the PA acoustic effect. The entire field of view of the US transducer is illuminated by pulsed-laser radiation of the desired wavelength. A major advantage of this approach is the possibility of superimposing the PA image with a conventional US image, as switching between the two imaging modalities can easily be implemented. The combination of US and PA imaging has been intensively investigated by several groups in the past several years (135, 136). The combination of

these two techniques can also be small enough to fit into a catheter measuring a few millimeters in diameter (137).

Instead of piezo-based pressure detection, several arrangements of optical interferometric detectors have been presented. Laufer et al. (138) used a 2D sensor plate based on interferences on a thin polymer film on top of a glass plate that is brought in direct contact with the sample. The PA pressure wave compresses the film and thus influences the interference between the front and back sides of the polymer film. A probe beam is scanned over this sensing plate (138). A similar approach uses a fiber-based (139) or open-beam (140) Mach-Zehnder interferometer. These approaches have not yet been used for quantitative measurements, but they bear the potential of revealing chromophore concentrations with high spatial resolution when combined with suitable image-reconstruction algorithms (141). A recent development in PAT is Doppler PA, where the PA wave undergoes a Doppler shift when the absorbing structure generating the PA wave moves relative to the acoustic detector (142). Flow-velocity measurements of absorbing nanoparticles were possible for values as low as 0.055 mm s^{-1} with the described setup.

5.8. Contrast Agents for Medical Imaging

Contrast in DOT as well as in other tomographic approaches based on optical absorption can be greatly enhanced by using additional contrast agents. A typical agent for medical imaging is indocyanine green (ICG), which features strong absorption between 600 nm and 900 nm while emitting fluorescence between 750 nm and 950 nm (143). Alternative contrast agents for absorption-based tomographic methods are metallic nanoparticles, particularly gold or silver particles in a size range around 20 nm. Absorption of these particles can exceed the values of ICG by a factor of 40,000, the optical properties can be tailored to the specific requirements, and they can be surface-functionalized to bind specifically to a binding partner such as tumor cells (144). Other than ICG, no other nanoparticles have yet been certified for medical applications, and toxicity may be an issue.

When a selective fluorescence marker is employed for tomography, the background fluorescence of the biological matrix limits the contrast. Although the optical properties of the chosen fluorophore can be tailored to minimize this effect, it cannot be eliminated completely. Thus, reconstruction of fluorescence DOT may present an extremely ill-posed problem. Improvement is possible by using up-converting labels, as significant anti-Stokes emission is hardly observed as wideband emission background (145).

6. PERSPECTIVE

The number of OT techniques has significantly increased over the past decade. A literature research on the keywords "optical tomography" provided 26 hits for 1990, 719 for 2000, and 9,202 for 2010. With an increasing number of applications, the number of different imaging modalities is also increasing. Extrapolating current trends, the coming years will bring an increase in the number of hyphenated techniques, which reveal different optical and chemical parameters in parallel. When considering the major fields of tomographic developments, atmospheric and biomedical imaging, the top priorities are better spatial resolution in combination with high temporal resolution. For highly scattering media, as commonly considered in medicine, local scattering and absorption properties have to be analyzed in parallel. These parameters are required for quantitative analysis of physiological parameters such as blood oxygenation and hemoglobin concentration. These activities are aiming for a real-time analysis of physiological parameters with a spatial resolution down to the cellular or even subcellular resolution. The use of tomographic contrast enhancers,

such as nanoparticles with tailored optical properties, is one way to meet these requirements. The particles can be functionalized for specific applications such as tumor-cell labeling.

New applications for OT will also be observed in industrial process control because of their potential to lead to optimized production processes. In atmospheric tomography, global climate analysis will present future challenges for tomographic analyses with high spatial resolution. These applications will also require increased sensitivity and precision, providing optimized databases for local and global climate modeling.

DISCLOSURE STATEMENT

The author is not aware of any affiliations, memberships, funding, or financial holding that might be perceived as affecting the objectivity of this review.

LITERATURE CITED

1. Ferrando M, Spiess WEL. 2000. Review: confocal scanning laser microscopy. A powerful tool in food science. *Food Sci. Technol. Int.* 6:267–84
2. Stachs O, Guthoff RF, Zhivov A. 2009. In vivo confocal microscopy, an inner vision of the cornea: a major review. *Clin. Exp. Ophthalmol.* 37:100–17
3. McGhee CNJ, Patel DV. 2009. In vivo confocal microscopy of human corneal nerves in health, in ocular and systemic disease, and following corneal surgery: a review. *Br. J. Ophthalmol.* 93:853–60
4. Arridge RS. 1999. Optical tomography in medical imaging. *Inverse Probl.* 15:R41–93
5. Van Tiggelen R. 2002. In search for the third dimension: from radiostereoscopy to three-dimensional imaging. *J. Belge Radiol. Belgisch Tijdschr. Radiol.* 85:266–70
6. Arridge SR, Schweiger M. 1997. Image reconstruction in optical tomography. *Philos. Trans. R. Soc. Lond. Ser. B* 352:717–26
7. Egger H, Schlottbom M. 2011. Efficient reliable image reconstruction schemes for diffuse optical tomography. *Inverse Probl. Sci. Eng.* 19:155–80
8. Kolehmainen V, Arridge SR, Vauhkonen M, Kaipio JP. 2000. Simultaneous reconstruction of internal tissue region boundaries and coefficients in optical diffusion tomography. *Phys. Med. Biol.* 45:3267–83
9. Hadamard J. 1902. Sur les problèmes aux dérivées partielles et leur signification physique. *Princeton Univ. Bull.* 13:49–52
10. Wang L, Jacques LS, Zheng L. 1995. MCML: Monte Carlo modeling of light transport in multi-layered tissues. *Comput. Methods Progr. Biomed.* 47:131–46
11. Song Z, Dong K, Hu XH, Lu JQ. 1999. Monte Carlo simulation of converging laser beams propagating in biological materials. *Appl. Opt.* 38:2944–49
12. Keijzer M, Jacques LS, Prahl SA, Welch AJ. 1989. Light distribution in artery tissue: Monte Carlo simulation for finite-diameter laser beams. *Lasers Surg. Med.* 9:148–54
13. Chu M, Vishwanath K, Klose AD, Dehghani H. 2009. Light transport in biological tissue using three-dimensional frequency-domain simplified spherical harmonics equations. *Phys. Med. Biol.* 54:2493–509
14. Groenhuis RAJ, Ferwerda AH, Ten Bosch JJ. 1983. Scattering and absorption of turbid materials determined from reflection measurements. 1. Theory. *Appl. Opt.* 22:2456–62
15. Cong W, Shen H, Cong A, Wang Y, Wang G. 2007. Modeling photon propagation in biological tissues using a generalized Delta-Eddington phase function. *Phys. Rev. E* 76:051913
16. Wang VL, Wu H-I. 2007. *Biomedical Optics: Principle and Imaging*. Hoboken, NJ: Wiley
17. Gao F, Niu H, Zhao H, Zhang H. 1998. The forward and inverse models in time-resolved optical tomography imaging and their finite-element method solutions. *Image Vis. Comput.* 16:703–12
18. Arridge RS, Hebden CJ, Schwinger, et al. 2000. A method for three-dimensional time-resolved optical tomography. *Int. J. Imaging Syst. Technol.* 11:2–11
19. Jin M, Jiao Y, Gao F, Zhao H. 2010. A finite difference solution to 2-dimensional radiative transfer equation for small-animal imaging. *Proc. SPIE* 7557:75570S

20. Radon J. 1917. Über die Bestimmung von Funktionen durch ihre Integralwerte längs gewisser Mannigfaltigkeiten. *Berl. Verh. Sächsis. Wiss. Leipzig* 69:262–77
21. Bracewell NR, Preston WG. 1956. Radio reflection and refraction phenomena in the high solar corona. *Astrophys. J.* 123:14–29
22. Bracewell NR. 1990. Numerical transforms. *Science* 248:697–704
23. Chan HP, Hadjiiski L, Zhou C, Sahiner B. 2008. Computer-aided diagnosis of lung cancer and pulmonary embolism in computed tomography: a review. *Acad. Radiol.* 15:535–55
24. Wang Y, Xing D. 2003. Optical projection tomography: theory and optimization. *Alt. Int. Conf. Adv. Laser Technol. Biomed. Opt.* 5486:67–71
25. Wedberg CT, Stamnes JJ, Singer W. 1995. Comparison of the filtered back-propagation and the filtered back-projection algorithms for quantitative tomography. *Appl. Opt.* 34:6575–81
26. Pan CX, Sidky YE, Vannier M. 2009. Why do commercial CT scanners still employ traditional, filtered back-projection for image reconstruction? *Inverse Probl.* 25:123009
27. Darrell A, Meyer H, Marias K, Brady M, Ripoll J. 2008. Weighted filtered back-projection for quantitative fluorescence optical projection tomography. *Phys. Med. Biol.* 53:3863–81
28. Devaney JA. 1987. A fast-filtered back-propagation algorithm for ultrasound tomography. *IEEE Trans.* 34:330–40
29. Wedberg CT, Stamnes JJ. 1996. Recent results in optical diffraction microtomography. *Meas. Sci. Technol.* 7:414–18
30. Gordon R, Bender R, Herman TG. 1970. Algebraic reconstruction techniques (ART) for three-dimensional electron microscopy and X-ray photography. *J. Theor. Biol.* 29:471–81
31. Brendel B, Ziegler R, Nielsen T. 2008. Algebraic reconstruction techniques for spectral reconstruction in diffuse optical tomography. *Appl. Opt.* 47:6392–403
32. Correia DP, Ferrao P, Caldeira-Pires A. 2000. Flame three-dimensional tomography sensor for in-furnace diagnostics. *Proc. Combust. Inst.* 28:431–38
33. Hino M, Aono T, Nakajima M, Yuta S. 1987. Light-emission computed-tomography system for plasma diagnostics. *Appl. Opt.* 26:4742–46
34. Liu LH, Li BX. 2002. Inverse radiation problem of axisymmetric turbulent sooting free flame. *J. Quant. Spectrosc. Radiat. Transf.* 75:481–91
35. Wan X, Yu LS, Cai G, Gao Y, Yi J. 2004. Three-dimensional plasma field reconstruction with multiobjective optimization emission spectral tomography. *J. Opt. Soc. Am. Opt. Image Sci. Vis.* 21:1161–71
36. Panne U, Clara M, Haisch C, Niessner R. 1998. Analysis of glass and glass melts during the vitrification of fly and bottom ashes by laser-induced plasma spectroscopy. Part II. Process analysis. *Spectrochim. Acta B* 53:1969–81
37. Panne U, Haisch C, Clara M, Niessner R. 1998. Analysis of glass and glass melts during the vitrification process of fly and bottom ashes by laser-induced plasma spectroscopy. Part I: Normalization and plasma diagnostics. *Spectrochim. Acta B* 53:1957–68
38. Goursat E. 1903. On a problem of inversion resolved by Abel. *Acta Math.* 27:129–33
39. Quintero MC, Alvarez R, Rodero A. 2002. An Abel inversion method for radially resolved measurements in the axial injection torch. *Spectrochim. Acta B* 57:1665–80
40. Shabanov SV, Gornushkin IB. 2011. Emission plasma tomography with large acceptance angle apertures relevant to laser induced plasma spectroscopy. *Spectrochim. Acta B* 66:413–20
41. Makabe T. 1997. Robot-assisted optical emission tomography in a CCP and ICP. *Phys. Ioniz. Gases* 18:257–68
42. Debal F, Wautelet M, Dauchot JP, Hecq M. 1997. Tomography of optical emission line intensities of a radio-frequency magnetron discharge. *Appl. Spectrosc.* 51:1340–45
43. Xiong J, Zhang GJ, Gao HM, Wu L. 2011. Reconstruction of emission coefficients for a non-axisymmetric coupling arc by algebraic reconstruction technique. *J. Quant. Spectrosc. Radiat. Transf.* 112:92–99
44. Schielke W, Rottig G, Bandlow I, Pickalov V, Ohl A. 1997. On the capability of spectrally resolved optical emission tomography for the diagnostic of nonisothermal low-pressure technological plasmas. *Surf. Coat. Technol.* 97:742–48

45. Colbeck I, Lazaridis M. 2010. Aerosols and environmental pollution. *Naturwissenschaften* 97:117–31
46. Johansson M, Galle B, Rivera C, Zhang Y. 2009. Tomographic reconstruction of gas plumes using scanning DOAS. *Bull. Volcanol.* 71:1169–78
47. Baum RT, McGrattan KB, Nyden MR. 1998. An examination of the applicability of computed tomography for the measurement of component concentrations in fire-generated plumes. *Combust. Flame* 113:358–72
48. Basha SB, Reddy MS, Joshi HV, Jha B. 2005. Evaluation of the emission characteristics of trace metals from coal and fuel oil fired power plants and their fate during combustion. *J. Hazard. Mater.* 123:242–49
49. Hashmonay RA, Varma RM, Modrak MT, Kagann RH, Segall RR, Sullivan PD. 2008. Radial plume mapping: a US EPA test method for area and fugitive source emission monitoring using optical remote sensing. *Adv. Environ. Monit.* 1:21–36
50. Byer LR, Shepp AL. 1979. Two-dimensional remote air-pollution monitoring via tomography. *Opt. Lett.* 4:75–77
51. Wolfe DC, Byer RL. 1982. Model studies of laser-absorption computed-tomography for remote air-pollution measurement. *Appl. Opt.* 21:1165–78
52. Seinfeld HJ, Pandis NS. 1998. *Atmospheric Chemistry and Physics*. New York: Wiley
53. Koch B. 2010. Status and future of laser scanning, synthetic aperture radar and hyperspectral remote sensing data for forest biomass assessment. *ISPRS J. Photogramm. Remote Sens.* 65:581–90
54. Pirotti F. 2011. Analysis of full-waveform LIDAR data for forestry applications: a review of investigations and methods. *iFor. Biogeosci. For.* 4:100–6
55. Fischer ML, Price PN, Thatcher TL, Schwalbe CA, Craig MJ, et al. 2001. Rapid measurements and mapping of tracer gas concentrations in a large indoor space. *Atmos. Environ.* 35:2837–44
56. Drescher CA, Gadgil JA, Price, et al. 1996. Novel approach for tomographic reconstruction of gas concentration distributions in air: use of smooth basis functions and simulated annealing. *Atmos. Environ.* 30:929–40
57. Yan L, Xu HQ, Xue R, Wang XF, Ren YB, et al. 2005. Path concentration distribution of toluene using remote sensing FTIR and one-dimensional reconstruction method. *J. Environ. Sci. Health A* 40:183–91
58. Verkruysse W, Todd LA. 2005. Novel algorithm for tomographic reconstruction of atmospheric chemicals with sparse sampling. *Environ. Sci. Technol.* 39:2247–54
59. Wu FC, Chen LY, Chen CC, Yang TT, Chang PE. 2007. Applying open-path Fourier transform infrared spectroscopy for measuring aerosols. *J. Environ. Sci. Health A* 42:1131–40
60. Platt U, Stutz J. 2008. *Differential Optical Absorption Spectroscopy Principles and Applications*. Heidelberg: Springer
61. Pundt I. 2006. DOAS tomography for the localisation and quantification of anthropogenic air pollution. *Anal. Bioanal. Chem.* 385:18–21
62. Pundt I, Mettendorf KU. 2005. Multibeam long-path differential optical absorption spectroscopy instrument: a device for simultaneous measurements along multiple light paths. *Appl. Opt.* 44:4985–94
63. Mettendorf KU, Hartl A, Pundt I. 2006. An indoor test campaign of the tomography long path differential optical absorption spectroscopy technique. *J. Environ. Monit.* 8:279–87
64. Belotti C, Cuccoli F, Facheris L, Vaselli O. 2003. An application of tomographic reconstruction of atmospheric CO2 over a volcanic site based on open-path IR laser measurements. *IEEE Trans. Geosci. Remote Sens.* 41:2629–37
65. Honninger G, Platt U. 2002. Observations of BrO and its vertical distribution during surface ozone depletion at Alert. *Atmos. Environ.* 36:2481–89
66. Honninger G, von Friedeburg C, Platt U. 2004. Multi axis differential optical absorption spectroscopy (MAX-DOAS). *Atmos. Chem. Phys.* 4:231–54
67. Frins E, Bobrowski N, Platt U, Wagner T. 2006. Tomographic multiaxis-differential optical absorption spectroscopy observations of Sun-illuminated targets: a technique providing well-defined absorption paths in the boundary layer. *Appl. Opt.* 45:6227–40
68. Louban I, Piriz G, Platt U, Frins E. 2008. Measurement of SO_2 and NO_2 applying ToTaL-DOAS from a remote site. *J. Opt. A* 10:104017
69. Lim K, Treitz P, Wulder M, St-Onge B, Flood M. 2003. LIDAR remote sensing of forest structure. *Progr. Phys. Geogr.* 27:88–106

70. Wang K, Franklin ES, Guo X, Cattet M. 2010. Remote sensing of ecology, biodiversity and conservation: a review from the perspective of remote sensing specialists. *Sensors* 10:9647–67
71. Butts J. 1997. Atmospheric tomography using differential absorption LIDAR. *Proc. SPIE* 2956:30–38
72. Grant WB. 1991. Differential absorption and Raman LIDAR for water-vapor profile measurements: a review. *Opt. Eng.* 30:40–48
73. Tratt DM, Whiteman DN, Demoz BB, Farley RW, Wessel JE. 2005. Active Raman sounding of the Earth's water vapor field. *Spectrochim. Acta A* 61:2335–41
74. Alados-Arboledas L, Muller D, Guerrero-Rascado JL, Navas-Guzman F, Perez-Ramirez D, Olmo FJ. 2011. Optical and microphysical properties of fresh biomass burning aerosol retrieved by Raman LISAR, and star and Sun photometry. *Geophys. Res. Lett.* 38:01807
75. Borg LA, Holz RE, Turner DD. 2011. Investigating cloud radar sensitivity to optically thin cirrus using collocated Raman LIDAR observations. *Geophys. Res. Lett.* 38:05807
76. Sassen K. 1991. The polarization LIDAR technique for cloud research: a review and current assessment. *Bull. Am. Meteorol. Soc.* 72:1848–66
77. Sassen K. 2003. Polarization in LIDAR: a review. *Proc. SPIE* 5158:151–60
78. Gurdev LL, Dreischuh NT, Stoyanov VD. 1998. Pulse back-scattering tomography based on LIDAR principle. *Opt. Commun.* 151:339–52
79. Sharpe J, Ahlgren U, Perry P, Hill B, Ross A, et al. 2002. Optical projection tomography as a tool for 3D microscopy and gene expression studies. *Science* 296:541–45
80. Wong MD, Henkelman RM. 2011. 3D volumetric ex-vivo mouse embryo imaging and image registration using MRI, micro-CT and optical projection tomography. *Dev. Biol.* 356:177–77
81. Walls RJ, Sled GJ, Sharpe J, Henkelman RM. 2007. Resolution improvement in emission optical projection tomography. *Phys. Med. Biol.* 52:2775–90
82. Sharpe J. 2003. Optical projection tomography as a new tool for studying embryo anatomy. *J. Anat.* 202:175–81
83. Miao Q, Yu J, Rahn JR, Meyer MG, Neumann T, et al. 2010. Dual-mode optical projection tomography microscope using gold nanorods and hematoxylin-stained cancer cells. *Opt. Lett.* 35:1037–39
84. Thomas A, Bowsher J, Roper J, Oliver T, Dewhirst M, Oldham M. 2010. A comprehensive method for optical-emission computed tomography. *Phys. Med. Biol.* 55:3947–57
85. Ouakli N, Guevara E, Dubeau S, Beaumont E, Lesage F. 2010. Laminar optical tomography of the hemodynamic response in the lumbar spinal cord of rats. *Opt. Express* 18:10068–77
86. Hillman EMC, Boas DA, Dale AM, Dunn AK. 2004. Laminar optical tomography: demonstration of millimeter-scale depth-resolved imaging in turbid media. *Opt. Lett.* 29:1650–52
87. Yuan S, Li Q, Jiang J, Cable A, Chen Y. 2009. Three-dimensional coregistered optical coherence tomography and line-scanning fluorescence laminar optical tomography. *Opt. Lett.* 34:1615–17
88. McBride TO, Pogue BW, Gerety ED, Poplack SB, Osterberg UL, Paulsen KD. 1999. Spectroscopic diffuse optical tomography for the quantitative assessment of hemoglobin concentration and oxygen saturation in breast tissue. *Appl. Opt.* 38:5480–90
89. Duck AF. 1990. *Physical Properties of Tissue: A Comprehensive Reference Book*. London: Academic
90. Bai J, Wang DF, Liu X, Liu F. 2010. Full-angle fluorescence diffuse optical tomography with spatially coded parallel excitation. *IEEE Trans. Inf. Technol. Biomed.* 14:1346–54
91. Franceschini MA, Toronov V, Filiaci ME, Gratton E, Fantini S. 2000. On-line optical imaging of the human brain with 160-ms temporal resolution. *Opt. Express* 6:49–57
92. Farsiu S, Christofferson J, Eriksson B, Milanfar P, Friedlander B, et al. 2007. Statistical detection and imaging of objects hidden in turbid media using ballistic photons. *Appl. Opt.* 46:5805–22
93. Liang XP, Jiang HB. 2004. Experimental studies of near-infrared diffuse optical tomography in turbid media: distributed excitation source and periodical boundary conditions coefficient. *J. Opt. Pure Appl. Opt.* 6:454–60
94. Ntziachristos V, Chance B. 2001. Probing physiology and molecular function using optical imaging: applications to breast cancer. *Breast Cancer Res.* 3:41–46
95. Pogue BW, Patterson MS, Jiang H, Paulsen KD. 1995. Initial assessment of a simple system for frequency-domain diffuse optical tomography. *Phys. Med. Biol.* 40:1709–29

96. Jiang HB, Zhang QZ. 2005. Three-dimensional diffuse optical tomography of simulated hand joints with a 64x64-channel photodiodes-based optical system. *J. Opt. Pure Appl. Opt.* 7:224–31
97. Proskurin SG. 2011. Using late arriving photons for diffuse optical tomography of biological objects. *Quantum Electron.* 41:402–6
98. Mansfield JR. 2010. Distinguished photons: a review of in vivo spectral fluorescence imaging in small animals. *Curr. Pharm. Biotechnol.* 11:628–38
99. Gao F, Jin M, Jiao YT, Poulet P, Zhang LM, Zhao HJ. 2010. A comparative investigation on linear inversion schemes in fluorescence lifetime tomography. *Proc. SPIE* 7557:75570N; doi: 10.117/12.834835
100. Sakhalkar SH, Dewhirst M, Oliver T, Cao Y, Oldham M. 2007. Functional imaging in bulk tissue specimens using optical emission tomography: fluorescence preservation during optical clearing. *Phys. Med. Biol.* 52:2035–54
101. Huang D, Swanson AE, Lin CP, Schuman JS, Stinson WG, et al. 1991. Optical coherence tomography. *Science* 254:1178–81
102. Bouman EB, Tearney JG. 2001. *Handbook of Optical Coherence Tomography*. New York: Marcel Dekker
103. Fercher AF. 2010. Optical coherence tomography: development, principles, applications. *Z. Med. Phys.* 20:251–76
104. Hariprasad SM, Kiernan DF, Mieler WF. 2010. Spectral-domain optical coherence tomography: a comparison of modern high-resolution retinal imaging systems. *Am. J. Ophthalmol.* 149:18–31
105. Chang SD, Mao YX, Flueraru C, Sherif S. 2008. Optical coherence tomography: technology and applications. *Proc. SPIE* 7 156:715606–9
106. Roth EJ, Kozak JA, Yazdanfar S, Rollins AM, Izatt JA. 2001. Simplified method for polarization-sensitive optical coherence tomography. *Opt. Lett.* 26:1069–71
107. Koch E, Walther J, Cuevas M. 2009. Limits of Fourier domain Doppler-OCT at high velocities. *Sens. Actuators Phys.* 156:8–13
108. Meier C, Hermann B, Hofer B, Povazay B, Drexler W. 2009. Spectroscopy in single and double layered weakly scattering phantoms with frequency domain OCT. *Proc. SPIE* 7175:71750X
109. Kirillin MY, Priezzhev AV, Myllylä R. 2008. Effect of paper porosity on OCT images: Monte Carlo study. *Proc. SPIE* 7022:702214
110. Haisch C, Niessner R. 2007. Visualisation of transient processes in biofilms by optical coherence tomography. *Water Res.* 41:2467–72
111. Wagner M, Taherzadeh D, Haisch C, Horn H. 2010. Investigation of the mesoscale structure and volumetric features of biofilms using optical coherence tomography. *Biotechnol. Bioeng.* 107:844–53
112. Ju MJ, Lee SJ, Kim Y, Shin JG, Kim HY, et al. 2011. Multimodal analysis of pearls and pearl treatments by using optical coherence tomography and fluorescence spectroscopy. *Opt. Express* 19:6420–32
113. Lesaffre M, Farahi S, Gross M, Delaye P, Boccara AC, Ramaz F. 2009. Acousto-optical coherence tomography using random phase jumps on ultrasound and light. *Opt. Express* 17:18211–18
114. Wang LHV. 2001. Mechanisms of ultrasonic modulation of multiply scattered coherent light: a Monte Carlo model. *Opt. Lett.* 26:1191–93
115. Wang LHV. 2003. Ultrasound-mediated biophotonic imaging: a review of acousto-optical tomography and photo-acoustic tomography. *Dis. Markers* 19:123–38
116. Welch JA, van Gemert MJC, eds. 1995. *Optical-Thermal Response of Laser-Irradiated Tissue*. New York: Plenum Press. 925 pp.
117. Bratchenia A, Molenaar R, van Leeuwen TG, Kooyman RPH. 2011. Acousto-optic-assisted diffuse optical tomography. *Opt. Lett.* 36:1539–41
118. Bal G, Schotland JC. 2010. Inverse scattering and acousto-optic imaging. *Phys. Rev. Lett.* 104:043902
119. Atlan M, Forget BC, Ramaz F, Boccara AC, Gross M. 2005. Pulsed acousto-optic imaging in dynamic scattering media with heterodyne parallel speckle detection. *Opt. Lett.* 30:1360–62
120. Rousseau G, Blouin A, Monchalin JP. 2009. Ultrasound-modulated optical imaging using a confocal Fabry-Pérot interferometer and a powerful long pulse laser. *Opt. Lett.* 34:3445–47
121. Lai PX, Roy RA, Murray TW. 2009. Quantitative characterization of turbid media using pressure contrast acousto-optic imaging. *Opt. Lett.* 34:2850–52

122. Forget BC, Atlan M, Selb J, Pottier L, Ramaz F, Boccara AC. 2003. High-contrast FFT acousto-optical tomography of biological tissues with a frequency-chirped modulation of the ultrasound. *Biomed. Optoacoust.* 4960:147–55
123. Praeger M, Brocklesby WS, de Paula AM, Frey J, Baumberg JJ, et al. 2005. Generalised ultrafast dispersion scans of continuum generation induced by sub-50fs chirped pulses in highly nonlinear tapered planar waveguides. *Proc. SPIE* 5714:200–07
124. Sigrist WM. 1986. Laser generation of acoustic waves in liquids and gases. *J. Appl. Phys.* 60:R83–121
125. Patel NCK, Kerl JR. 1977. New optoacoustic cell with improved performance. *Appl. Phys. Lett.* 30:578–79
126. Haisch C, Zell K, Sperl J, Vogel MW, Niessner R. 2009. Quantitative analysis with the optoacoustic/ultrasound system OPUS. *Proc. SPIE* 7177:717702
127. Xu M, Wang VL. 2006. Photoacoustic imaging in biomedicine. *Rev. Sci. Instrum.* 77:041101/1–22
128. Wang VL. 2008. Prospects of photoacoustic tomography. *Med. Phys.* 35:5758–67
129. Pilatou MC, Voogd NJ, de Mul FFM, Steenbergen W, van Adrichem LNA. 2003. Analysis of three-dimensional photoacoustic imaging of a vascular tree in vitro. *Rev. Sci. Instrum.* 74:4495–99
130. Kolkman RGM, Hondebrink E, Steenbergen W, de Mul FFM. 2003. In vivo photoacoustic imaging of blood vessels using an extreme-narrow aperture sensor. *IEEE J. Sel. Top. Quantum Electron.* 9:343–46
131. Yuan Y, Yang HS, Xing D. 2010. Preclinical photoacoustic imaging endoscope based on acousto-optic coaxial system using ring transducer array. *Opt. Lett.* 35:2266–68
132. Zemp RJ, Song L, Bitton R, Shung KK, Wang LV. 2008. Realtime photoacoustic microscopy in vivo with a 30-MHz ultrasound array transducer. *Opt. Express* 16:7915–28
133. Oraevsky AA, Savateeva EV, Solomatin SV, Karabutov AA, Andreev VG, et al. 2002. Optoacoustic imaging of blood, for visualization and diagnostics of breast cancer. *Proc. SPIE* 4618:81–94
134. Manohar S, Kharine A, van Hespen JCG, Steenbergen W, van Leeuwen TG. 2005. The Twente Photoacoustic Mammoscope: system overview and performance. *Phys. Med. Biol.* 50:2543–57
135. Haisch C, Eilert-Zell K, Vogel MM, Menzenbach P, Niessner R. 2010. Combined optoacoustic/ultrasound system for tomographic absorption measurements: possibilities and limitations. *Anal. Bioanal. Chem.* 397:1503–10
136. Niederhauser JJ, Jaeger M, Lemor R, Weber P, Frenz M. 2005. Combined ultrasound and optoacoustic system for real-time high-contrast vascular imaging in vivo. *IEEE Trans. Med. Imaging* 24:436–40
137. Karpiouk BA, Wang B, Emelianov YS. 2010. Development of a catheter for combined intravascular ultrasound and photoacoustic imaging. *Rev. Sci. Instrum.* 81:014901
138. Laufer J, Zhang E, Raivich G, Beard P. 2009. Three-dimensional noninvasive imaging of the vasculature in the mouse brain using a high resolution photoacoustic scanner. *Appl. Opt.* 48:D299–306
139. Nuster R, Paltauf G, Ditlbacher H, Burgholzer P. 2008. Integrated waveguide sensor for acoustic wave detection in photoacoustic tomography. *Proc. SPIE* 6856:68560E
140. Paltauf G, Nuster R, Haltmeier M, Burgholzer P. 2007. Photoacoustic tomography using a Mach-Zehnder interferometer as an acoustic line detector. *Appl. Opt.* 46:3352–58
141. Burgholzer P, Matt GJ, Haltmeier M, Paltauf G. 2007. Exact and approximative imaging methods for photoacoustic tomography using an arbitrary detection surface. *Phys. Rev. E* 75:046706
142. Wang VL, Fang H, Maslov K. 2007. Photoacoustic doppler effect from flowing small light-absorbing particles. *Phys. Rev. Lett.* 99:184501
143. Intes X, Ripoll J, Chen Y, Nioka S, Yodh AG, Chance B. 2003. In vivo continuous-wave optical breast imaging enhanced with Indocyanine Green. *Med. Phys.* 30:1039–47
144. Islam T, Harisinghani MG. 2009. Overview of nanoparticle use in cancer imaging. *Cancer Biomarkers* 5:61–67
145. Xu CT, Axelsson J, Andersson-Engels S. 2009. Fluorescence diffuse optical tomography using upconverting nanoparticles. *Appl. Phys. Lett.* 94:251107

Annual Review of
Analytical Chemistry

Volume 5, 2012

Contents